Multiple Modes on Embedded Inverted Microstrip Lines

George E. Ponchak, *Senior Member, IEEE* and Manos M. Tentzeris, *Member, IEEE*

G. E. Ponchak is with the NASA Glenn Research Center, Cleveland, OH 44135 USA
M. M. Tentzeris is with the Georgia Institute of Technology, Atlanta, GA 30332-0250 USA

***Abstract* — Embedded transmission lines are commonly used in silicon radio frequency integrated circuits to reduce insertion loss and decrease circuit size. In this paper, experimental measurements and Finite Difference Time Domain (FDTD) analysis are used to show that embedded inverted microstrip lines are not suitable for use above a few GHz.**

***Index Terms* — microstrip, inverted microstrip, MMIC, multi-layer circuits.**

I. Introduction

Silicon Radio Frequency Integrated Circuits (SiRFICs) have matured greatly over the past five years and are now found in a multitude of commercial products. These commercial products have primarily relied on lumped element (inductor, capacitor, and resistor) circuit design to minimize circuit size and the associated fabrication cost. However, inductors are still problematic with low quality factor and self resonant frequency, and inductor layout is still being optimized to lessen the effects of eddy currents in the silicon substrate. Furthermore, interconnect losses are still high. The copper (Cu)-damascene process was developed to partially solve these problems. In the Cu-damascene process, multiple layers of SiO_2 are grown on top of the Si substrate and Cu metal lines are embedded in the SiO_2 [1]. This multi-layer circuit build-up has also been employed on Si and GaAs substrates with polyimide and BCB to build smaller circuits with lower loss at microwave and millimeter-wave frequencies [2]-[5]. These multi-layer circuits for RFICs consist of 2 to 20 μm thick layers of SiO_2, polyimide, BCB, or a similar insulator deposited over the GaAs or Si substrate after the active circuits are fabricated on the semiconductor. Within each layer of insulator, Au, Cu, or Al metal traces may be deposited, and with vertical interconnects between the layers, a three dimensional circuit is built.

Flexibility in circuit layout is possible because different types of thin film transmission lines may easily be integrated together. Within the multi-layer structure, thin film microstrip (TFMS) shown in Fig. 1a [1], [6]-[9]; inverted microstrip shown in Fig. 1d [1]-[3],[8]; stripline shown in Fig. 1b [2]; and coplanar waveguide (CPW) shown in Fig. 1c [1],[6], [10] have been demonstrated. The propagation constant ($\gamma=\alpha+j\beta$) of thin film microstrip embedded in polyimide on a silicon substrate has been experimentally measured from 1 to 110 GHz, and no evidence of higher order modes was reported [6], [9]. In [1], [6], and [10], coplanar waveguide on or embedded in an insulator over a silicon substrate were characterized and the measured β is reported to be single mode through 40 GHz. However, embedded inverted microstrip lines have not been shown to be single moded and low loss.

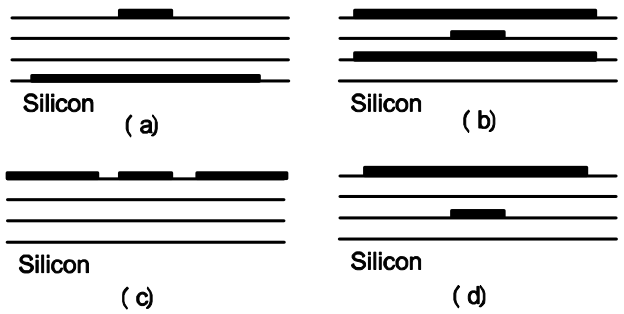

Figure 1: Embedded transmission lines on silicon substrate: (a) Thin Film Microstrip, (b) stripline, (c) coplanar waveguide, (d) inverted microstrip.

Experimental measurements of embedded inverted microstrip have only been reported through 20 GHz [1], [3], [8]. After an initially high propagation constant ($\beta=\omega\,\varepsilon_{eff}^{0.5}/c$ where ε_{eff} is the effective permittivity) for frequencies below a few GHz, ε_{eff} of the transmission line should be constant or slightly increasing with frequency if a single, quasi-TEM mode is supported by the transmission line. However, in Fig. 3 of [8], a noticeable change in ε_{eff} is seen at 16 GHz, and a very high measured attenuation (α) of 28 dB/cm at 20 GHz is reported. The stated reason for theses properties is leakage of electromagnetic fields into the Si substrate. In Fig. 10 of [1], a lower α is reported for inverted microstrip, and α appears to be only marginally dependent on the Si resistivity. However, it is noted that the slope of α with frequency varies with Si resistivity, and α does not vary as $f^{0.5}$ or $f^{1.0}$ as expected for conductor or dielectric loss respectively, implying another loss mechanism.

In this paper, embedded inverted microstrip lines on 20 Ω-cm Si are experimentally characterized from 1 to 50 GHz. Anomalous characteristics are presented for the first time and attributed to coupling to dominant surface wave leakage modes. Finite Difference Time Domain (FDTD) analysis is presented to confirm the experimental measurements.

 0-7803-9472-0/06/$20.00©2006 IEEE

II. Experimental Measurement Procedure

Embedded inverted microstrip lines are fabricated on silicon wafers of 20 Ω-cm resistivity and thickness of 529 μm. Four 2.5 μm thick layers of PI-2611 polyimide are deposited. PI-2611 polyimide has a relative permittivity of 3.12 measured at 1 MHz and a loss tangent of 0.002 measured at 1 kHz. The embedded metal lines consist of 0.02 μm of Cr, 1.5 μm of Au and 0.02 μm of Cr while the metal lines on top of the polyimide consist of 200 μm of Cr and 1.5 μm of Au.

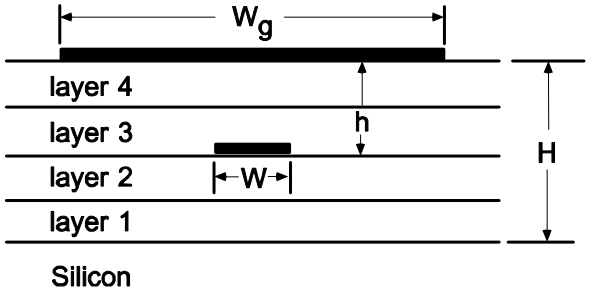

Figure 2: Cross sectional cut of inverted microstrip line.

Fig. 2 shows a cross sectional cut through the embedded inverted microstrip line. The total polyimide thickness is 10 μm, and transmission lines are fabricated on layers 1, 2, and 3 with a characteristic impedance (Zc) of 50 Ω that were determined from Sonnet 2-D field solutions. In each case, the ground plane width is five times the strip width. Table 1 summarizes the inverted microstrip lines.

Table 1: Dimensions of embedded inverted microstrip lines.

Layer	h (μm)	W (μm)	W_g (μm)	Zc (Ω)
1	7.5	11	55	50
2	5.0	9	45	50
3	2.5	5	25	50

CPW probe pads designed for 150 μm pitch probes are used to transition from the coaxial transmission lines of the vector network analyzer to the substrate. The transition between the CPW probe pads and the inverted microstrip is shown in Fig. 3. The CPW ground planes merge to form a single ground plane on the upper surface of polyimide, while the center conductor of the probe pads terminates in a vertical via hole that connects to the strip of the inverted microstrip. The distance between the probe contact region and the via hole is 150 μm, the via hole diameter is 15 μm, and the distance from the merged ground plane to the via hole is 50 μm.

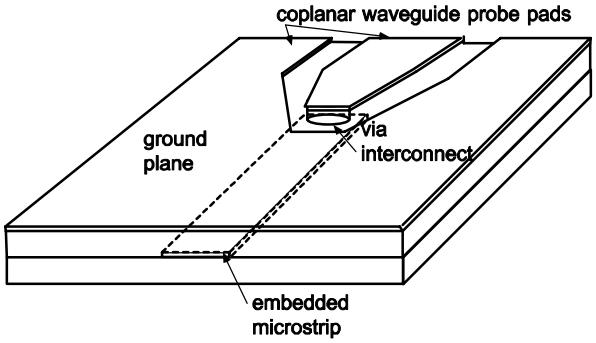

Figure 3: Transition from CPW probe pads to embedded inverted microstrip.

It is noted that this transition between CPW and microstrip and/or inverted microstrip has been successfully used over a wide frequency range [11], [12]. It has been reported that resonances within the CPW to microstrip transition can be established if the dimensions are large relative to the wavelength [13]. Specifically, if the length from the end of the CPW center line to the via hole or the length from the end of the microstrip to the via hole is greater than 1 mm for a substrate permittivity of 9.2, resonances are expected in the frequency range from 1 to 50 GHz. For the lines reported here, the overlap distance is less than 0.02 mm, which accounts for fabrication errors and design tolerances and the substrate permittivity is 3.12. Thus, resonances due to the transition are not expected. Lastly, the transition in Fig. 3 is opposite to the transition used in [9] in which the ground planes were embedded and via holes transitioned the CPW probe pad ground planes to the embedded ground plane while the strip remained on the upper surface. In [9], no resonances or issues with multiple modes were reported from 1 to 110 GHz.

The embedded inverted microstrip lines are characterized using two procedures. In the first, a through-reflect-line (TRL) calibration is performed with delay line lengths of 850, 1700, 3500, and 10000 μm using the NIST software program *Multical*. *Multical* calculates the complex propagation constant of a single moded transmission line from the excess data gathered during the vector network analyzer system calibration. Furthermore, the reference plane is established in the center of the through line so the effects of the probe pads and the transition from CPW to inverted microstrip are removed. In the second set of measurements, the system is calibrated to the probe pads using open-short-load calibration standards provided by GGB Industries and:

$$A = \frac{(1 - S_{11})(1 + S_{22}) - S_{21}S_{12}}{2S_{12}}$$

$$\gamma = \alpha + j\beta = \frac{1}{L}\ln(A \pm \sqrt{A^2 - 1})$$

where L is the total line length is used to determine γ.

III. Measured Inverted Microstrip Characteristics

The measured α and ε_{eff} for 50 Ω embedded inverted microstrip lines on 20 Ω-cm Si substrate are shown in Figs. 4 and 5 respectively. First, it is noted that while not in quantitative agreement, there is qualitative agreement between the results obtained from the TRL calibration and those obtained by calibrating to the probe tips. There are several irregular characteristics noted. First, the attenuation increases at a rate greater than expected if only conductor loss were present or if only dielectric losses were present, greater than $f^{0.5}$ and $f^{1.0}$ respectively. Typically, this is an indication of attenuation due to radiation into either surface or space waves. Second, there is a frequency region of decreasing attenuation, for which there is no physical explanation, but interference between multiple modes on a transmission line does yield characteristics similar to that shown in Fig. 4. The measured ε_{eff} also exhibits a large change in slope within small frequency regions, which is an indication that the propagation mode has changed.

IV. Finite Difference Time Domain Analysis

The full-wave FDTD technique was used for the theoretical mode decomposition of the inverted microstrip lines. The E- and H-field components are implemented in a leapfrog configuration. An adaptive grid with neighboring cell aspect ratio smaller or equal to 2 maintains a second-order global accuracy. Numerical meshes of 100x100x120 cells terminated with 10 PML cells in each direction provide accurate results for a time-step of 0.99 the Courant limit. A Gaussian pulse with f_{max}=60 GHz was applied vertically as a soft source close to the front-end of the microstrip, and its values get superimposed on the FDTD calculated field value for all cells in the excitation region for each time-step. The FDTD analysis is capable of mapping the electric and magnetic fields of the inverted microstrip lines and separating them into the various modes by using cross-sectional probes for specific frequencies and identifying the differentiating features of the different modes.

The total electric field for two modes of an embedded inverted microstrip line on layer 2 with a strip width of 9 μm is shown in Fig. 6. In both figures, the propagation constant is 750 rad/m and ε_{eff} is 3.16 and 3.96 in Figs. 6a and 6b respectively. It is clear that the desired microstrip mode is shown in Fig. 6a, and its ε_{eff} of 3.16 is the expected value for a microstrip line embedded in a homogeneous material with a relative permittivity of 3.12. Fig. 6b shows a higher order mode with significant electric field penetration into the Si substrate, but the total field strength is 20 dB below the microstrip mode strength. FDTD analysis confirms other modes with higher values of ε_{eff} that are at least 20 dB below the microstrip mode.

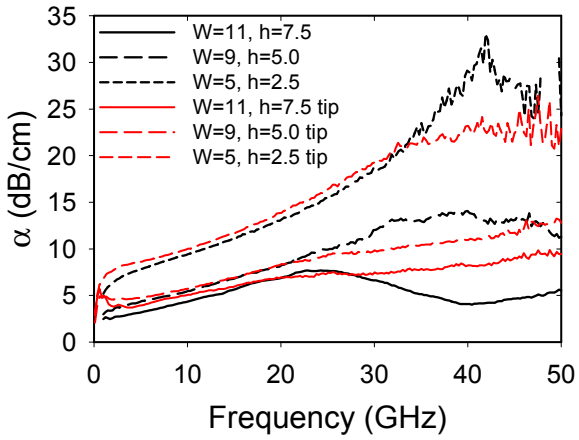

Figure 4: Measured attenuation of 50 Ω embedded inverted microstrip lines on 20 Ω-cm Si.

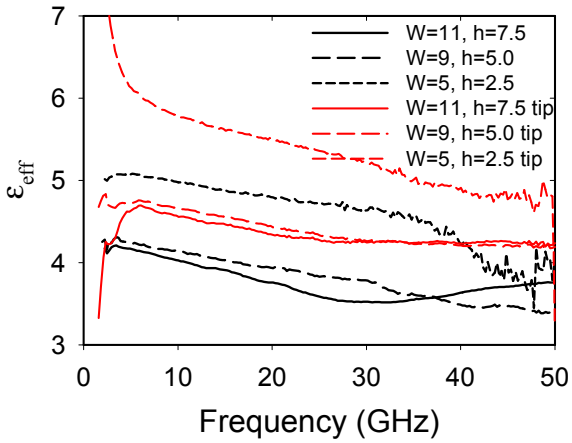

Figure 5: Measured effective permittivity of 50 Ω embedded inverted microstrip lines on 20 Ω-cm Si.

V. Discussion

If there is a ground plane on the bottom of the Si wafer as there is for most circuits, especially packaged circuits, there are a total of three independent conductors that can support two independent fundamental modes. One mode is obviously the desired microstrip mode that is shown in Fig. 6a. The second mode may be thought of as an asymmetric stripline mode or a quasi-microstrip mode between the upper and lower ground planes. These modes are predicted by FDTD and Sonnet to have an ε_{eff} of approximately 7 and 4 respectively at 20 GHz. However,

FDTD analysis confirms that these modes are very weakly excited by the dominant microstrip mode, and the electric fields for the mode shown in Fig. 6b, which has an ε_{eff} of approximately 4 at 20 GHz, is not a microstrip like mode. Instead, FDTD analysis confirms that a leaky wave mode is excited in X-Band, which leaks power away at an angle from the microstrip line. Furthermore, it is known that there is a strong coupling between the inverted microstrip mode and the leaky wave mode, which gives rise to effects as seen in Figs 4 and 5.

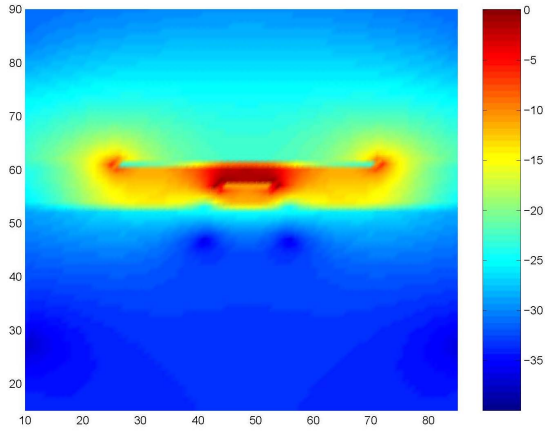

(a)

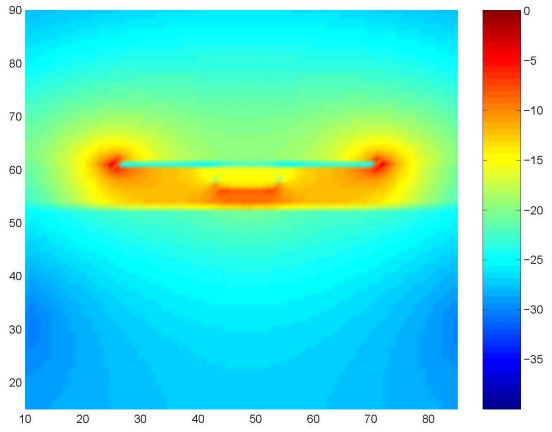

(b)

Figure 6: Total electric field for two modes on a 50 Ω embedded inverted microstrip line on layer 2.

VI. Conclusion

In this paper, we have shown that the measured propagation constant of embedded inverted microstrip shows indications of higher order modes and significant coupling between the different modes. The source of these modes is not the transition between CPW and the microstrip line. For the resistivity of the Si wafers, the skin depth is greater than the Si thickness; thus, the higher order modes are not due to a parasitic stripline mode. Lastly, the FDTD analysis confirms the existence of these higher order modes. Because these modes are easily coupled to the desired microstrip mode, embedded inverted microstrip is not a suitable transmission line for Si RFICs.

References

[1] J. N. Burghartz, D. C. Edelstein, K. A. Jenkins, and Y. H. Kwark, "Spiral inductors and transmission lines in silicon technology using copper-damascene interconnects and low-loss substrates," *IEEE Trans. Microwave Theory Tech.*, Vol. 45, No. 10, pp. 1961-1968, Oct. 1997.

[2] S. Banba and H. Ogawa, "Small-sized MMIC amplifiers using thin dielectric layers," *IEEE Trans. Microwave Theory Tech.*, Vol. 43, pp. 485–492, March 1995.

[3] H. Ogawa, T. Hasegawa, S. Banba, and H. Nakamoto, "MMIC transmission lines for multi-layered MMIC's," IEEE MTT-S Int. Microwave Symp. Dig., pp. 1067–1070, June, 1991.

[4] T. Tokumitsu, T. Hiraoka, H. Nakamoto, and T. Takenaka, "Multilayer MMIC using a 3 μm X 3-layer dielectric film structure," *IEEE MTT-S Int. Microwave Symp. Dig.*, pp. 831–834, May 1990.

[5] T. Hiraoka, T. Tokumitsu, and M. Aikawa, "Very small wide-band MMIC magic T's using microstrip lines on a thin dielectric film," *IEEE Trans. Microwave Theory Tech.*, Vol. MTT-37, pp. 1569–1575, Oct. 1989.

[6] G. E. Ponchak, "RF transmission lines on silicon substrates," *29 th European Microwave Conference Dig.*, Munich, Germany, Oct. 5-7, 1999, pp. 158-161.

[7] B. Piernas, K. Nishikawa, K. Kamogawa, T. Nakagawa, and K. Araki, "High-Q factor three-dimensional inductors," *IEEE Trans. Microwave Theory Tech.*, Vol. 50, No. 8, pp. 1942-1949, Aug. 2002.

[8] W. Ryu, S.-H. Baik, H. Kim, J. Kim, M. Sung, and J. Kim, "Embedded microstrip interconnection lines for gigahertz digital circuits," *IEEE Trans. Advanced Packaging,* Vol. 23, No. 3, pp. 495-503, Aug. 2000.

[9] G. E. Ponchak and A. N. Downey, "Characterization of thin film microstrip lines on polyimide," *IEEE Trans. Components, Packaging, and Manufacturing Tech. -Part B*, Vol. 21, No. 2, pp. 171-176, May 1998.

[10] G. E. Ponchak and L. P. B. Katehi, "Measured attenuation of coplanar waveguide on CMOS grade silicon substrates with a polyimide interface layer," *IEE Electronics Letters*, Vol. 34, No. 13, pp. 1327-1329, June 25, 1998.

[11] B. Golja, H. B. Sequeira, S. Duncan, G. Mendenilla, and N. E. Byer, "A coplanar-to-microstrip transition for W-band circuit fabrication with 100-μm-thick GaAs wafers," *IEEE Microwave and Guided Wave Letters*, Vol. 3, No. 2, pp. 29-31, Feb. 1993.

[12] J.-G. Yook, N. I. Dib, and L. P. B. Katehi, "Characterization of high frequency interconnects using finite difference time domain and finite element methods," *IEEE Trans. Microwave Theory and Tech.*, Vol. 42, No. 9, pp. 1727-1736, Sept. 1994.

[13] H. Jin, R. Vahldieck, J. Huang, and P. Russer, "Rigorous analysis of mixed transmission line interconnects using the frequency-domain TLM method," *IEEE Trans. Microwave Theory and Tech.*, Vol. 41, No. 12, pp. 2248-2255, Dec. 1993.

[14] H. Hasegawa, M. Furukawa, and H. Yanai, "Properties of microstrip line on Si-SiO2 system," *IEEE Trans. Microwave Theory and Tech.*, Vol. MTT-19, No. 11, pp. 869-881, Nov. 1971.